Nanoscale Horizons

COMMUNICATION

View Article Online
View Journal

Making metal surfaces strong, resistant, and multifunctional by nanoscale-sculpturing†

M. Baytekin-Gerngross, M. D. Gerngross, J. Carstensen and R. Adelung*

Cite this: DOI: 10.1039/c6nh00140h

Received 29th July 2016,
Accepted 30th August 2016

DOI: 10.1039/c6nh00140h

rsc.li/nanoscale-horizons

Surfaces are the crucial and limiting factor in nearly all metal applications, especially when technologically relevant alloys are employed. Insufficient surface properties on the nano- and micro-scale of metals determine, *e.g.* metal–polymer composite stability, implant biocompatibility, or corrosion resistance. Conventional surface preparation is just like an arbitrary cut through the metal body optimized for bulk behavior so that such surfaces contain various element mixtures and complex microstructures in which grains and lattice planes vary in their chemical stability from weak to strong. In contrast, the here described novel nanoscale-surface sculpturing based on semiconductor etching knowledge turns surfaces of everyday metals into their most stable configuration, but leaves the bulk properties unaffected. Thus, nanoscale-sculpturing ensures stronger, reliable joints to nearly all materials, reduces corrosion vastly, and generates a multitude of multifunctional surface properties not limited to those shown below.

Conceptual insights

3D nanoscale-sculptured surfaces consist nearly entirely of stable native oxide covered grains and thus resemble most stable mechanical and chemical surfaces/interfaces in addition to the nearly optimal topology for interlocking structures to other materials. Conventional chemical surface treatments remove defects being specific to the surface (*e.g.* saw damage, mechanical damage after sand blasting, mechanical polishing, or even damages induced by ion implantation), etch out (selectively) grain boundaries, form metal oxide layers on the surface, thus having mostly an intrinsically 2D-character. In strong contrast to nearly all relevant technical surface treatments on metals and semiconductors, the sculpturing approach utilizes the intrinsic features of the surface-near grain structure on the nanoscale. The (electro-)chemistry is tuned to selectively etch out entire or at least large parts of grains on the nanolevel in a coordinated manner introducing an intrinsic micro 3D-character into the resulting surfaces. Deep cavities with undercuts allowing for mechanical interlocking are thus an intrinsic feature of sculpturing. Due to the 3D-character the preserved grains, plains, and facets, *i.e.*, the bulk structure is extremely stable, since, *e.g.*, no grain boundaries are widened weakening the surface microstructure.

Metals and metal alloys possess a huge range of applications each having certain requirements on the surface. Adhesive properties,[1–4] biocompatibility,[5–7] or corrosion resistance,[8–10] are just some important demands, since metal surfaces are typically either in contact with liquid/gaseous media or directly joined to other materials. Thus, many metals/alloys obtain their technical relevance mainly from their passivating native oxide layers. Real world metals are typically polycrystalline and their surfaces contain, *e.g.* mechanical surface damage, alloying elements *etc.* On these spots the formation of native oxide layers be slower, less stable, or adhere worse compared to ideal single crystals. These metal oxides, *i.e.* like TiO_2, Al_2O_3, or ZnO, perfectly coat and adhere tightly to their metal surface,[5,11,12] and behave with respect to their electrochemical properties like wide-band gap semiconductors. They are chemically stable, show stronger crystallographic anisotropy, and enable much higher selective control of their (electro-)chemical dissolution. Such dissolution control on the nanoscale can be done on metal-oxide–semiconductors, *e.g.* by tuning the Fermi level and/or density of surface states. For the here introduced wet chemical metal surface sculpturing, the decisive idea is to fine-tune the intermediate oxide formation on the metal surface and its subsequent dissolution. This emphasizes these grains and planes oxidizing slowest during sculpturing leaving a surface that allows for a native oxide coverage with the same surface characteristics on the entire sculptured metal surface. Thus sculpturing creates the most stable metal surfaces.

Even though anodic dissolution reactions take place on the metal surface during sculpturing, it should not be called anodization. This term is misleading, because anodization is a tool and does not describe what is done and what the result is. Well-known typical results of anodization are the formation of thick oxide layer on metal surfaces,[13] defect etching with the preferential dissolution of defected surface areas,[14,15] and

Institute for Materials Science, Kiel University, Kaiserstr. 2, 24143 Kiel, Germany. E-mail: ra@tf.uni-kiel.de; Fax: +49 431 880 6124; Tel: +49 431 880 6116

† Electronic supplementary information (ESI) available. See DOI: 10.1039/c6nh00140h

eventually electropolishing with the formation of smooth surfaces by using a chemistry being insensitive to *e.g.* surface-near structural defects or chemical composition of surface-near grains.[16,17]

Obviously none of these processes describe the here introduced process. To emphasize the difference the term sculpturing was introduced. Speaking in electrochemical terms, the sculpturing process means having the right balance between direct (defect etching) and indirect dissolution (electropolishing). This offers simultaneously a defined control over the surface topography and chemical composition in the surface-near regions. Thus, the metal/metal alloy sculpturing allows to design surface properties widely independent from their bulk properties, like enhanced corrosion resistance.

As one of the most decisive differences to all other typical metal etchants acting as defect etchants,[18–21] sculpturing *via* semiconductor dissolution on the nanoscale enables complete suppression of the conventionally observed preferential grain boundary dissolution, so that a mechanical weakening of the surface-near grain structure is prevented. Of course a sculptured metal surface still contains lattice defects, but exhibits smooth faceted surfaces on a sub-micrometer scale reflecting the crystal orientation of the grains. In summary, sculpturing is insensitive to grain boundaries (like electropolishing) and sensitive to crystal orientations and chemical compositions (like defect etching) and thus results in unique surface topologies.

Other metal surface structuring techniques like plasma treatment,[22] laser ablation,[23,24] or subtractive manufacturing techniques like grit-blasting[25] show principle limitations because they are insensitive to crystal orientations.

Obtaining the most stable metal surfaces can be achieved by two distinct pathways of chemical sculpturing as depicted in Fig. 1a – in all sketches *z* indicates the surface normal. The first can be described as a special kind of chemical dealloying (enhancing chemical surface purity) being very successful for sculpturing Ti/Ti alloys.

The second pathway is crystallographic etching splitting into two branches, anisotropic chemical etching and anisotropic electrochemical etching. Anisotropic chemical etching results in sculptured surfaces for Al/Al alloys. Essentially, even though similar Al surface geometries are known,[26] their extreme stability and other properties are unknown so far. The anisotropic electrochemical etching pathway proved to be very efficient for sculpturing Zn surfaces.

Fig. 1b describes schematically the time evolution of surface sculpturing *via* the three sculpturing pathways. For Ti, the first etching step is to chemically smoothen the surface defect structure making it easy accessible for preferential etching in the second step. The sculptured surface develops under highly selective chemical dissolution of the electrochemically more instable parts (light grey) as shown in the sketch of Fig. 1b. These parts include intermetallic phases like Ti_3Al, precipitates, inclusions, dislocation networks, *etc.* The resulting sculptured surface consists of hole-like cavities in various shapes and with undercuts in various sizes. The sculptured Al structure develops by formation and controlled dissolution of ultra-thin Al-oxide

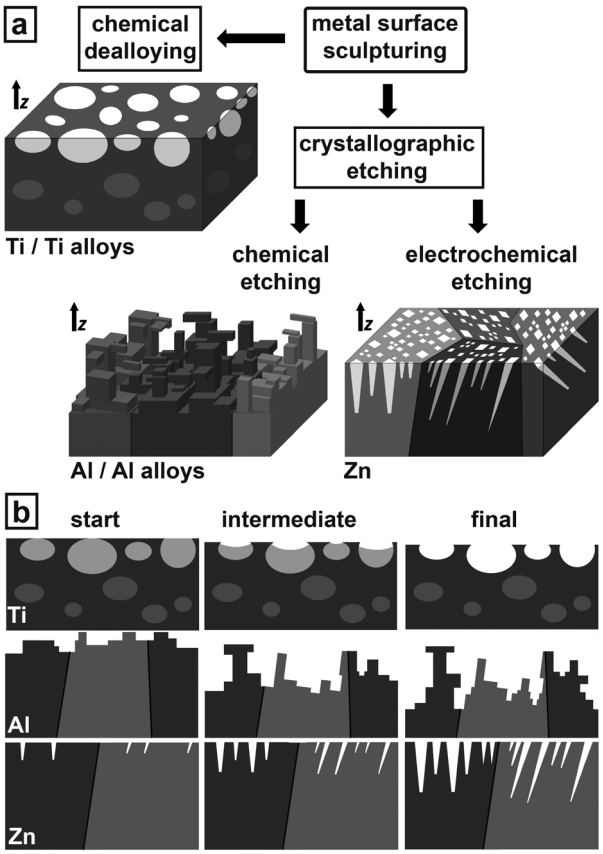

Fig. 1 Schematic images of sculptured metal surfaces. (a) Strategy for sculpturing metal surfaces, and (b) the time evolution of the metal surface during sculpturing. For Ti, the dark grey areas indicate the Ti bulk matrix. The mid grey spots correspond to parts being electrochemically more instable compared to the bulk Ti matrix, but are inaccessible to preferential dissolution unlike the light grey ones. For Al and Zn, the diverse grey shades indicate different grain orientations, the black lines grain boundaries.

layers resulting in step-like and freestanding structures. In Zn crystallographically-oriented pores grow by highly anisotropic electrochemical dissolution at the pore tips along selected crystallographic directions, while the pore walls are partially passivated against dissolution. Different crystal orientations at the surface lead to growth of domains with pores parallel aligned to each other showing highest corrosion resistance.

The formation of the surfaces schematically shown in Fig. 1 is not an experimental result found by coincidence, but a general feature which can be applied to all metals which possess stable metal oxides, as we have shown with the examples of different sculptured metals being presented in Fig. 2. All experimental data about the formation of the sculptured metal surfaces, their characterization and the characterization of their properties can be found in the ESI† under 'materials and methods'. For demonstrating the relevance of sculpturing, only commercially available metals/metal alloys are employed.

Nanoscale-sculpturing generates the most stable metal surfaces as shown for Ti-grade 2 (medical applications) and Ti-3Al-2.5V (marine applications) in Fig. 2a and b as representatives for further Ti alloys (referring to Fig. S1, ESI†).

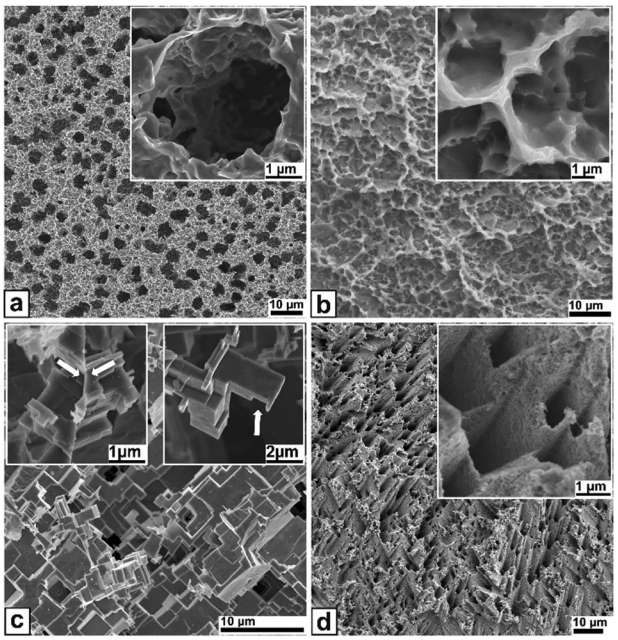

Fig. 2 Top view SEM images on various etch-sculptured metal surfaces. (a) Ti-grade 2, (b) Ti-3Al-2.5V, (c) AA5754, and (d) Zn 99.95%. The insets show high magnifications of characteristic features. All experimental data can be found in the ESI† under 'materials and methods'.

Sculptured Ti-grade 2 surfaces possess a high density of hole-like cavities. They are roundish with a typical micrometer-range diameter and corrugated openings having nanometer-range undercuts as key feature for mechanical interlocking with, *e.g.* polymers. Additionally, the surface exhibits a superimposed rather spiky nanostructure. For Ti-3Al-2.5V the cavities are smaller in diameter and shallower compared to Ti-grade 2, but also exhibit the undercut openings. The inset shows the intergrowth of single cavities creating broader structures with walls containing even smaller sized cavity-like structures increasing the undercuts further. The EDX-maps (see Fig. S7, ESI†) suggest a preferential dissolution of Al-rich parts from the bulk matrix. This is a clear sign that sculpturing dissolves electrochemically related to the α-phase, since elements like Al and O are well-known α-stabilizers.[27]

Fig. 2c depicts the chemically-sculptured surface of AA5754 as a representative for other Al alloys (referring to Fig. S2 and S3, ESI†). The surface consists of cuboid elements with nearly perfectly flat faces which are oriented 90° to each other forming a six-fold symmetry. In fcc crystals like Al only {100} planes provide these characteristics. The cuboid sizes range from tens of nanometers up to several micrometers. Depending on the grain orientation the cuboids are tilted towards each other. The insets give the key parameters of the sculptured surface with a grain boundary being preserved during sculpturing on the left proving no preferential etching of grain boundaries and a freestanding structure on the right. In contact to, *e.g.*, polymers they act as hooks highly improving adhesion under mechanical load, see examples in Fig. 3.

In Fig. 2d the electrochemically-sculptured Zn surface is shown with pore arrays grown under various angles into Zn depending on the crystal orientations of the surface, from perpendicular to almost parallel to *z*.

The inset is a close-up on such a domain exhibiting the parallel alignment of pores within a domain. Typically, the pore shape is a distorted hexagon transforming into a rhomboid for larger pores. Pore diameters range from ~100 nm to several microns. X-ray diffractograms and EDX-maps of sculptured Ti-3Al-2.5V, AA5754, and Zn surfaces (Fig. S4–S9, ESI†) suggest, if indeed, just native oxide coverage of the sculptured metal surfaces, but no thick oxide layers as known from anodic metal oxidization.[13]

The fundamental problem of many types of joints is adhesive failure. This is solved for metal–polymer joints by nanoscale-sculpturing of the metal surfaces, as such composites displayed only cohesive failure in all performed mechanical tests.

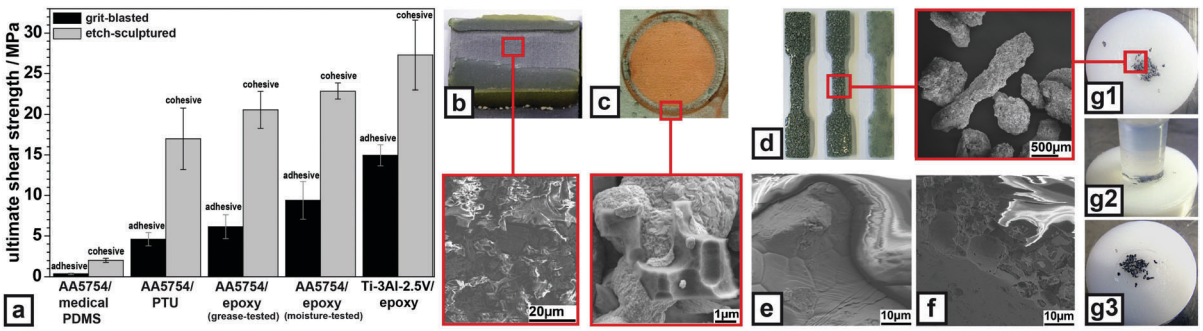

Fig. 3 Adhesion properties of etch-sculptured metal surfaces. (a) single-lap-shear tests of sandwich composites based on sculptured AA5754, resp. Ti-3Al-2.5V and various polymers showing mean USS including standard deviation (further illustration Videos S13 and S14, ESI†). (b) Fracture surface of sculptured AA5754–epoxy composite after moisture exposure and subsequent lap-shear-test, inset: high-magnification SEM image at indicated position. (c) AA5754–Cu joint made by galvanic Cu-deposition, inset: high-magnification SEM image at indicated position. (d) Dog bone-shaped composites based on sculptured Al micro-particles and PTU (left), EVA (middle), and epoxy resin (right), inset: SEM image of sculptured Al micro-particles before embedding. Close-up SEM image of the fracture surface of (e) an untreated Al micro-particle–PTU composite and (f) a sculptured Al micro-particle–PTU composite. (g1) Adhesive-free joining of POM–EVA *via* sculptured Al micro-particles partially impressed into POM, (g2) formed joint, (g3) after tensile testing; further illustration in Video S15, ESI.† All experimental data can be found in the ESI† under 'materials and methods'.

Fig. 3a demonstrates these adhesive properties of sculptured AA5754 and Ti-3Al-2.5V surfaces in connection with different polymer types forming sandwich composites. Grit-blasted surfaces of the same metals were used as reference. The here presented ultimate shear strength values (USS) are a conservative measure for the adhesion performance, since single-lap-shear tests always include peeling effects. Sculptured metal surfaces drastically increase the USS in all investigated joints. Sculptured composites fail exclusively cohesive, grit-blasted ones adhesively. For medical-grade polydimethylsiloxane (PDMS) the USS rises by a factor of 5.5 (from 0.36 MPa to 2 MPa). A similar result is found for polythiourethane (PTU) with a USS of 4.6 MPa (grit-blasted) to 17 MPa (sculptured) and for epoxy resins from 9.65 MPa (grit-blasted) to 21.5 MPa (sculptured). Grease on the to-be-glued surfaces is a typical source for adhesive joint failure.[28] As fingerprint simulation surface-greasing by conventional gear oil reveals no effect on the USS for sculptured AA5754 surfaces compared to gear-oil-free epoxy-resin-glued sculptured surfaces (21.5 MPa *vs.* 20.6 MPa), while grit-blasted surfaces exhibit a drastic reduction (from 9.65 MPa down to 6.13 MPa). Besides grease, moisture/environmental stability of joints is a crucial issue,[29] especially for anodized surfaces covered with thick oxide layers as obtained by standard anodizing.[13] The USS of grit-blasted and sculptured surfaces, indicates no degradation under moisture exposure (grit-blasted 9.39 MPa, sculptured 22.87 MPa). The slightly higher USS for sculptured surfaces could be explained by enhanced polymer-curing during moisture exposure, since the temperature under moisture exposure is above the used epoxy curing temperature. For sculptured Ti-3Al-2.5V surfaces, the same behavior is observed as for AA5754 with epoxy resins (grit-blasted 14.95 MPa, sculptured 27.3 MPa). The USS is higher compared to AA5754 because the peeling influence during single-lap-shear testing is diminished (higher Young's modulus, higher metal sheet thickness). As a typical representative the photograph in Fig. 3b provides a macroscopic view on the fracture surface of such a joint with a sculptured AA5754 surface. On first glance it might suggest a mixture of adhesive and cohesive failure with adhesive failure in between the polymer covered spots (yellowish top and bottom). The SEM image at the red-squared spot reveals the fracture to be directly above the sculptured surface, but within the polymer exhibiting cohesive failure.

Fig. 3c shows sculptured metal surfaces are also able to efficiently join various metals, *e.g.* Al and Cu as typical representatives of most problematic metal joints. The Cu film grows directly on the sculptured AA5754 surface completely enclosing the freestanding hooks and step-like AA5754 structures, see inset of Fig. 3c, without forming intermetallics like $CuAl_2$, CuAl, *etc.* deteriorating the electrical and mechanical properties as done by welding.[30] In the final stage these structures are overgrown forming a rigid connection between the Cu film and the AA5754 substrate. Compared to grit-blasted AA5754 where the Cu film partially detaches from the substrate on slight scratching, only the scratch without any detachment is visible being considered as cohesive failure (Fig. S10, ESI†).

Besides bulk materials even micro-particles with arbitrary shapes and sizes can be successfully sculptured (Fig. S3, ESI†). These sculptured micro-particles offer a multitude of applications, *e.g.* forming metal particle–polymer composites. As matrix material any polymer-type and various filling factors are possible, see Fig. 3d. Conventional metal particle–polymer composites suffer from reduced tensile strength due to adhesive failure at the particle/polymer interface resulting in reduced mechanical properties compared to the pure polymer.[31] The fracture surface of such an Al particle–PTU composite after tensile testing is depicted in Fig. 3e showing clearly adhesive failure at the particle–PTU interface. The fracture surface of such a sculptured Al particle–PTU composite (Fig. 3f) shows cohesive failure. The adhesion between the sculptured Al particles and the PTU matrix is so strong that the embedded Al particle is even torn apart, which shows the highest reachable adhesion.

Sculptured particles are also useful for adhesive-free joining of immiscible polymers with, *e.g.* very low surface energy. For such a joint, sculptured Al micro-particles are employed as linkers being partially imprinted into the heat-softened polyoxymethyl-ene (POM) surface (Fig. 3g1). The softened ethylen-vinylacetate (EVA) is now pressed on top of them forming the joint (Fig. 3g2). Tensile testing results in cohesive failure within the EVA slightly above the imprinted micro-particles (Fig. 3g3), while POM–EVA joints without micro-particles fail adhesively, as wells as when unsculptured particles are employed as linkers. Sculptured Al micro-particles can also be employed as linkers under compressive loads without fracture. Additionally, to thermoplasts, thermosets can also be joined adhesive-free *via* sculptured Al micro-particles in the same manner as described in ref. 32 and 33.

Besides these adhesion properties sculptured metal surfaces possess further remarkable properties making them multifunctional. In contact with seawater the sculptured AA5754 surface almost instantaneously reaches a quasi steady-state open-circuit potential of about −0.46 V (Fig. 4a), while no quasi steady-state is reached for the untreated polished AA5754 within 15 min. Comparing to the untreated AA5754, the quasi steady-state open-circuit potential of the sculptured AA5754 is shifted significantly towards a less corrosive potential by at least 80 mV. This means sculptured surfaces have a higher corrosion resistance. Under forced anodic corrosion (6.4 mA cm^{-1}) both surfaces react with a potential jump shifting the potential of the sculptured AA5754 only to a slightly higher value of about −0.42 V, since almost all spots on this surface are perfectly sculptured. As only a very low spot density on the sculptured surface is still actively corroding, the local current density is very high inducing a new-nucleation of active corrosion spots. With an increasing number of active corrosion spots the local current density strongly decays. Therefore, the voltage approaches its level before applying an anodic current. For the untreated surface the voltage approaches a nearly constant offset, since the forced corrosion current is distributed over the still very high density of active corrosion spots, so that the local current density increases only slightly.

Besides the above shown chemical pathway, the characteristic sculptured structure is also attainable by electrochemical

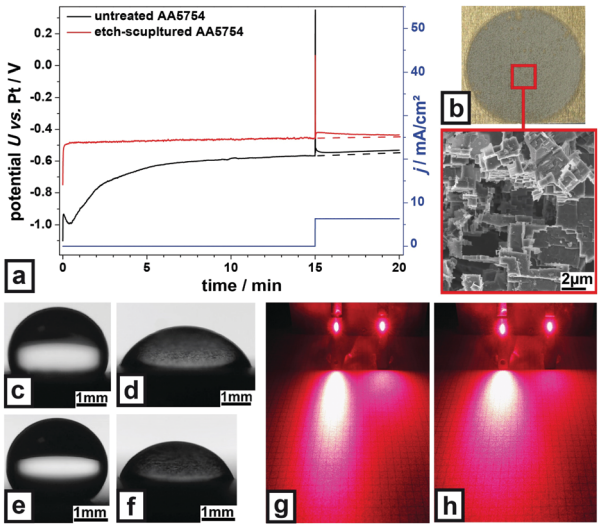

Fig. 4 Further properties of etch-sculptured metal surfaces. (a) Corrosion-test of untreated and etch-sculptured AA5754, (b) electrochemically-sculptured AA5754 in "green" chemistry, inset: high magnification SEM image at indicated position. Water droplets on (c) etch-sculptured and (d) grit-blasted Ti-3Al-2.5V, (e) etch-sculptured, and (f) grit-blasted AA5754; further illustration in Video S16, ESI.† Laser beam light scattering of (g) Ti-3Al-2.5V, grit-blasted (left), etch-sculptured (right), and (h) AA5754, grit-blasted (left) etch-sculptured (right). All experimental data can be found in the ESI† under 'materials and methods'.

etching (Fig. 4b). Unlike commonly used chromium containing electrolytes for anodizing Al[34] being highly poisonous and harmful to the environment, this method is very environment-friendly. This electrolyte emulates sea water containing only NaCl and Na_2SO_4. It is especially suitable for surface-sculpturing of large Al/Al alloy sheets with minimum material loss. Sculpturing influences also the surface wettability by water. Contact angle measurements reveal hydrophobic behavior for sculptured Ti-3Al-2.5V (Fig. 4c) with an average contact angle of 108.8° and moderate wettability (67.2°) for grit-blasted Ti-3Al-2.5V (Fig. 4d). Compared to sculptured Ti-3Al-2.5V, sculptured AA5754 (Fig. 4e) exhibits increased hydrophobicity with a contact angle of 138.8° and 71.6° for grit-blasted AA5754 (Fig. 4f). Sculptured surfaces react intelligently upon water exposure depending on the state of their native oxide layer. When it is mostly dehydrated, sculptured surfaces behave hydrophobic and water droplets roll off. In the hydrophobic state, sculptured surfaces even exhibit water jet reflection as shown in Video S11 (ESI†). When the oxide becomes hydrated, sculptured surfaces behave super-hydrophilic and water droplets spread facilitating evaporation. This process showed to be reversible.

In interaction with laser light sculptured metal surfaces offer completely different scattering properties. Exposed to red laser light sculptured Ti-3Al-2.5V (Fig. 3g) and AA5754 (Fig. 3h) surfaces display diffuse reflection barely illuminating the paper sheet used as screen, while grit-blasted surfaces show highly specular reflection. Compared to sculptured AA5754, sculptured Ti-3Al-2.5V exhibits less diffusive reflection. This diffuse reflectance behavior of sculptured surfaces showed to be independent from the wavelength of the incident laser beam and the incidence angle of the light.

Conclusions

In summary, the present work establishes an optimal route for enhancing the surface properties and functionalities of technically relevant metals/alloys keeping completely the beneficial mechanical bulk properties. Nanoscale-sculpturing exploits the right balance between direct and indirect dissolution producing remarkably corrosion-resistant surfaces (reaching a corrosion potential close to the pure metal) with a mechanical interlocking morphology without the conventional problem of preferential grain boundary dissolution. These sculptured metal surfaces are suitable for a huge variety of applications, *e.g.*, making gluing finally generally reliable in production of composites.

Acknowledgements

The authors thank Sören Kaps for his assistance in the contact angle measurements and Jörg Bahr for general technical assistance. Furthermore the authors thank Prof. Franz Faupel for helpful discussions and feedback on the manuscript.

References

1 A. J. Kinloch, *J. Mater. Sci.*, 1980, **15**, 2141.
2 F. Awaja, M. Gilbert, G. Kelly, B. Fox and P. J. Pigram, *Prog. Mater. Sci.*, 2009, **34**, 948.
3 W.-S. Kim, I.-H. Yun, J.-J. Lee and H.-T. Jung, *Int. J. Adhes. Adhes.*, 2010, **30**, 408.
4 H. Yuk, T. Zhang, S. Lin, G. A. Parada and X. Zhao, *Nat. Mater.*, 2016, **15**, 190.
5 M. Textor, C. Sittig, S. Tosatti and D. M. Brunette, in *Properties and biological Significance of natural oxide films on titanium and its alloys*, ed. D. M. Brunette, P. Tengvall, M. Textor and P. Thomsen, Springer, Germany, 2001, p. 171.
6 M. M. Stevens and J. H. George, *Science*, 2005, **310**, 1135.
7 M. Geetha, A. K. Singh, R. Asokamani and A. K. Gocia, *Prog. Mater. Sci.*, 2009, **54**, 397.
8 W. S. Miller, L. Zhuang, J. Bottema, A. Wittebrood, P. De Smet, A. Haszler and A. Vieregge, *Mater. Sci. Eng., A*, 2000, **280**, 37.
9 K. Lu, *Science*, 2010, **328**, 319.
10 W. Xu, N. Birbilis, G. Sha, Y. Wang, J. E. Daniels and Y. Xiao, *Nat. Mater.*, 2015, **14**, 1229.
11 C. E. Moffitt, D. M. Wieliczka and H. K. Yasuda, *Surf. Coat. Technol.*, 2001, **137**, 188.
12 J. Zuo and A. Erbe, *Phys. Chem. Chem. Phys.*, 2010, **12**, 11467.
13 J. D. Venables, *J. Mater. Sci.*, 1984, **19**, 2431.
14 H. Hanemann and A. Schrader, *Atlas Metallographicus Eine Lichtbildsammlung für die technische Metallographie Band I*, Gebrüder Bontraeger, Berlin, Germany, 1933.
15 E. Sirtl and A. Adler, *Z. Metallkd.*, 1961, **52**, 529.
16 T. P. Hoar and J. A. S. Mowat, *Nature*, 1950, **165**, 64.
17 D. R. Turner, *J. Electrochem. Soc.*, 1958, **105**, 402.
18 F. Variola, J. H. Yi, L. Richert, J. D. Wuest, F. Rosei and A. Nanci, *Biomaterials*, 2008, **29**, 1285.

19 T. D. Burleigh, in *Corrosion of aluminum and its alloys*, ed. G. E. Totten and D. S. MacKenzie, CRC Press, USA, 2003, p. 421.
20 J. A. Ramsey, *Nature*, 1950, **166**, 867.
21 A. D. Sheikh-Ali, D. A. Molodov and H. Garmestani, *Scr. Mater.*, 2002, **46**, 857.
22 U. Beck, R. Lange and H.-G. Neumann, *Biomol. Eng.*, 2007, **24**, 47–51.
23 B. K. Nayak and M. C. Gupta, *Opt. Laser Eng.*, 2010, **48**, 940–949.
24 A. Y. Vorobyev and C. Guo, *J. Appl. Phys.*, 2015, **117**, 033103.
25 C. Bockenheimer, B. Valeske and W. Possart, *Int. J. Adhes. Adhes.*, 2002, **22**, 349–356.
26 J. Yang, Z. Zhang, X. Xu, X. Men, X. Zhu and X. Zhou, *New J. Chem.*, 2011, **35**, 2422.
27 F. W. Wood and P. A. Romans, *Mater. Sci. Eng.*, 1972, **10**, 182–185.
28 G. Savage, *Eng. Failure Anal.*, 2007, **14**, 321.
29 A. J. Kinloch, *J. Mater. Sci.*, 1982, **17**, 617.
30 W.-B. Lee, K.-S. Bang and S.-B. Jung, *J. Alloys Compd.*, 2005, **390**, 212.
31 K. Strzelec and P. Pospiech, *Prog. Org. Coat.*, 2008, **63**, 133.
32 X. Jin, J. Strueben, L. Heepe, A. Kovalev, Y. K. Mishra, R. Adelung, S. N. Gorb and A. Staubitz, *Adv. Mater.*, 2012, **24**, 5676.
33 Nature Research Highlight, *Nature*, 2012, **489**, 9.
34 J. D. Venables, D. K. McNamara, J. M. Chen and T. S. Sun, *Appl. Surf. Sci.*, 1979, **3**, 88.

